Surface wave sensors based on nanometric layers of strongly absorbing materials

Yichen Zhang,[1] Christophe Arnold,[1] Peter Offermans,[2] and Jaime Gómez Rivas[1,3,*]

[1]*Center for Nanophotonics, FOM Institute AMOLF, c/o Philips Research Laboratories, High Tech Campus 4, 5656 AE Eindhoven, The Netherlands*
[2]*Holst Centre/IMEC-NL, High Tech Campus 31, 5656 AE Eindhoven, The Netherlands*
[3]*COBRA Research Institute, Eindhoven University of Technology, P.O. Box 513, 5600 MB Eindhoven, The Netherlands*
[*]*rivas@amolf.nl*

Abstract: We demonstrate the excitation of guided modes in thin layers of strongly absorbing chalcogenide glasses. These modes are similar to surface plasmon polaritons in terms of resonance width and shift with changes in the permittivity of the surrounding medium. We exploit these characteristics to demonstrate a high sensitivity chalcogenide glass refractive index sensor that outperforms gold surface plasmon resonance sensors at short wavelengths in the visible. This demonstration opens a new range of possibilities for sensing using different materials.

OCIS codes: (240.6690) Optics at surfaces, surface waves; (310.2785) Thin films, guided wave applications; (310.6860) Thin films, optical properties.

References and links

1. H. Raether, *Surface polaritons on smooth and rough surfaces and on gratings* (Springer-Verlag, 1988).
2. J. Homola, *Surface plasmon resonance based sensors* (Springer-Verlag, 2006).
3. X. Fan, I. M. White, S. I. Shopova, H. Zhu, J. D. Suter, and Y. Sun, "Sensitive optical biosensors for unlabeled targets: A review," Anal. Chim. Acta **620**, 8–26 (2008).
4. D. Sarid, "Long-range surface-plasma waves on very thin metal films," Phys. Rev. Lett. **47**, 1927–1930 (1981).
5. P. Berini, "Plasmon polariton waves guided by thin lossy metal films of finite width," Phys. Rev. B **61**, 10484–10503 (2001).
6. A. Boltasseva, T. Nikolajsen, K. Leosson, K. Kjaer, M. S. Larsen, and S. I. Bozhevolnyi, "Integrated optical components utilizing long-range surface plasmon polaritons," J. Lightwave Technol. **23**, 413–422 (2005).
7. P. Berini, "Long-range surface plasmon polaritons," Adv. Opt. Photon. **1**, 484–588 (2009).
8. K. Matsubara, S. Kawata, and S. Minami, "Multilayer system for a high precision surface plasmon resonance sensors," Opt. Lett. **15**, 75–77 (1990).
9. G. G. Nenningera, P. Tobiska, J. Homola, and S. S. Yee, "Long-range surface plasmons for high resolution surface plasmon resonance sensors," Sens. Act. B **74**, 145–151 (2001).
10. A. Kasry and W. Knoll, "Long range surface plasmon fluorescence spectroscopy," Appl. Phys. Lett. **89**, 101106 (2006).
11. J. Dostálek, A. Kasry, and W. Knoll, "Long range surface plasmons for observation of biomolecular binding events at metallic surfaces," Plasmonics **2**, 97–106 (2007).
12. G. J. Kovacs, "Surface polariton in the ATR angular spectra of a thin iron film bounded by dielectric layers," J. Opt. Soc. Am. **68**, 1325–1332 (1978).
13. F. Yang, J. R. Sambles, and G. W. Bradberry, "Long-range surface modes supported by thin films," Phys. Rev. B **44**, 5855–5872 (1991).
14. V. Giannini, Y. Zhang, M. Forcales, and J. Gómez Rivas, "Long-range surface polaritons in ultra-thin films of silicon," Opt. Express **16**, 19674–19685 (2008).

#162216 - $15.00 USD Received 1 Feb 2012; revised 27 Mar 2012; accepted 27 Mar 2012; published 10 Apr 2012

15. C. Arnold, Y. Zhang, and J. Gómez Rivas, "Long range surface polaritons supported by lossy thin films," Appl. Phys. Lett. **96**, 113108 (2010).
16. P. Yeh, *Optical waves in layered media* (John Wiley and Sons, 1988).
17. K. Okamoto, *Foundamentals of optical waveguides* (Elsevier, 2006).
18. L. H. Smith, M. C. Taylor, I. R. Hooper, and W. L. Barnes, "Field profiles of coupled surface plasmon-polaritons," J. Mod. Opt. **55**, 2929–2943 (2008).
19. J. Hu, V. Tarasov, A. Agarwal, L. Kimerling, N. Carlie, L. Petit, and K. Richardson, "Fabrication and testing of planar chalcogenide waveguide integrated microfluidic sensor," Opt. Express **15**, 2307–2314 (2007).
20. S. Raoux and M. Wuttig, *Phase change materials, science and applications* (Springer-Verlag, 2008).
21. K. Maex, M. R. Baklanov, D. Shamiryan, F. lacopi, S. H. Brongersma, and Z. S. Yanovitskaya "Low dielectric constant materials for microelectronics," J. Appl. Phys. **93**, 8793–8841 (2003).
22. A. Kruis, "Die äquivalentdisperision von starken elektrolyten in lösung," Z. Phys. Chem. B **34**, 13–50 (1936).
23. J. Gent, P. Lambeck, H. Kreuwel, and T. Popma, "Optimization of a chemooptical surface plasmon resonance based sensor," App. Opt. **29**, 2843–2849 (1990).
24. L. J. Sherry, S. -H. Chang, G. C. Schatz, and R. P. Van Duyne "Localized surface plasmon resonance spectroscopy of single silver nanocubes," Nano Lett. **5**, 2034–2038 (2005).
25. R. Jha and A. K. Sharma, "High-performance sensor based on surface plasmon resonance with chalcogenide prism and aluminum for detection in infrared," Opt. Lett. **34**, 749–751(2009).
26. M. Svedendahl, S. Chen, A. Dmitriev, and M. Käll, "Refractometric sensing using propagating versus localized surface plasmons: A direct comparison," Nano Lett. **9**, 4428–4433 (2009).
27. RIU stands for refractive index units. A *FoM* of 1 RIU^{-1} means that the resonance shifts 1 degree when the refractive index changes by 1.
28. P. B. Johnson and R. W. Christy, "Optical constants of the noble metals," Phys. Rev. B **6**, 4370–4379 (1972).

1. Introduction

A surface polariton is an electromagnetic wave coupled to a polarization excitation at the interface between two semi-infinite media. This polarization wave is called surface plasmon polariton (SPP) if one of the media is a metal and the other a non-absorbing dielectric [1]. Optical sensing based on surface plasmon polaritons is nowadays a broadly used technique for detecting small changes in the refractive index induced by analytes close to surfaces. These techniques have a high sensitivity associated to a strongly confined electromagnetic field close to the interface separating the metal from the non-absorbing dielectric. The field confinement allows for subwavelength optical detection [2]. A widely accepted characteristic of surface plasmon resonance sensors is that losses in the metal must be as low as possible to improve their sensitivity. Therefore, there is a small number of metals that is used for plasmonic sensing [3].

A recent development in surface polariton resonance (SPR) sensing is the use of ultra-thin metallic layers ($d < 50\,\mathrm{nm}$) embedded in a homogeneous medium. In the case of metals, these layers support the so-called long-range surface plasmon polaritons [4]. These surface modes suffer low loss due to the symmetry of the field with respect to the nanometric film, which reduces the electromagnetic energy stored in the lossy metal [5–7]. Since the spectral width of surface polariton resonances is proportional to the losses, much sharper resonances associated to long-range surface polaritons are observed in attenuated total internal reflection measurements [8]. These sharp resonances can improve the performance of optical sensors by increasing the detection resolution and the intrinsic sensitivity [9, 10]. Long-range surface polaritons have a longer decay length into the surrounding dielectric than surface polaritons, which arises from the coupling between the surface modes on opposite sides of the thin layer. The coupling strength can be tuned by varying the thickness of the metallic film, providing an easy tool to optimize the spatial overlap between the evanescent surface mode and the analyte under investigation. This optimization can increase significantly the sensitivity of surface plasmon resonance sensors [3].

Similar to long-range surface plasmon polaritons, it is possible to excite long-range guided modes in ultra-thin layers of strongly absorbing materials. These modes arise from the coupling of the evanescently decaying electromagnetic field, as a result of the strong absorption, at the

#162216 - $15.00 USD Received 1 Feb 2012; revised 27 Mar 2012; accepted 27 Mar 2012; published 10 Apr 2012

opposite sides of the thin layer. In spite of the similarities between long-range surface plasmon polaritons and long-range guided modes in absorbing thin films there are only a hand-full of articles about the last [12–15] and, to the best of our knowledge, none about optical sensing.

In this manuscript, we demonstrate that optical absorption in layers with a thickness of only a few nanometers can be an advantage for increasing the sensitivity of surface wave sensors. In particular, we show experimentally the efficient excitation of long-range guided modes in ultra-thin layers of strongly absorbing chalcogenide glasses and demonstrate a high sensitivity of these modes to changes in the refractive index of the surrounding medium. Long-range guided mode sensing can be easily extended to other materials, such as silicon, opening a new range of possibilities for sensing using materials that are compatible with CMOS technology.

The article is organized as follows: In section 2 we discuss the dispersion relation of guided modes in a thin slab with a transverse magnetic field component (TM-guided modes) and compare the case of a low-loss dielectric and a metallic waveguide with a waveguide of a strongly absorbing material. Measurements of the excitation of long-range guided modes in a thin layer of strongly absorbing chalcogenide glass are presented in section 3, demonstrating the shift of the resonance angle and width as a function of the index of refraction of the surrounding medium. In section 4 we derive the values of the intrinsic sensitivity and the decay length of surface modes in thin layer of materials with arbitrary permittivities. We also compare in this section the intrinsic sensitivities of thin film Au and chalcogenide glass sensors for different values of the thickness of the layer and the wavelength. The manuscript is ended with the conclusions.

2. Guided modes in absorbing thin layers

We consider here TM guided modes in a slab of a medium with permittivity ε_2 and thickness d in the z-direction, surrounded by a lossless dielectric characterized by the permittivity ε_1. These modes correspond to a magnetic field component oriented in the transverse direction to the slab, which we will take to be the y-direction. The dispersion relation of the TM guided modes can be split into two equations

$$\tanh\left(i\beta_{z2}d/2\right) = -\frac{\varepsilon_2\beta_{z1}}{\varepsilon_1\beta_{z2}}\,, \tag{1}$$

and

$$\tanh\left(i\beta_{z2}d/2\right) = -\frac{\varepsilon_1\beta_{z2}}{\varepsilon_2\beta_{z1}}\,, \tag{2}$$

where $\beta_{z1,2}^2 = \varepsilon_{1,2}k_0^2 - \beta_x^2$ is the mode wave number normal to the layer in medium 1 and 2, and β_x is the propagation constant or the wavenumber along the propagation direction. Equations (1) and (2) correspond to symmetric and antisymmetric TM modes in slab waveguides, where the symmetry refers to the H_y field component with respect to the middle plane of the slab.

By using the relation $\tanh(ix) = i\tan(x)$ and in the case of a thin layer of a non- or weakly absorbing dielectric, i.e., $\varepsilon_{2r} \gg \varepsilon_{2i} \simeq 0$, where ε_{2r} and ε_{2i} are the real and imaginary components of the permittivity of the thin layer, we can retrieve from Eqs. (1)-(2) the equations of the TM modes most commonly used in literature [16]. Note that these equations have multiple solutions defining the TM_m modes, where $m = 0, 1, 2...$ is the mode order or the number of nodes that the field has in the slab. The number of guided modes supported by the slab is determined by the ratio between its dimension and the wavelength [17]. If the thickness of the slab is much smaller than λ, only the symmetric fundamental mode, TM_0, can be guided by the dielectric slab. This mode does not have a cutoff frequency.

If we consider the slab formed by a non- or weakly absorbing metal, i.e., $|\varepsilon_{2r}| \gg \varepsilon_{2i} \simeq 0$, and $-\varepsilon_{2r} > \varepsilon_1$, Eq. (1) describes the so-called long-range surface plasmon polaritons (LRSPPs) and

#162216 - $15.00 USD Received 1 Feb 2012; revised 27 Mar 2012; accepted 27 Mar 2012; published 10 Apr 2012

Eq. (2) defines the short-range surface plasmon polaritons (SRSPPs). LRSPPs have a symmetric distribution of the normal component of the magnetic field H_z with respect to the middle plane of the slab, while short-range SRSPPs have an antisymmetric distribution of this normal magnetic field component [18]. These surface modes arise from the coupling between surface polaritons supported by the individual interfaces separating the thin layer and the surrounding dielectric. The different field symmetry between LRSPPs and SRSPPs can be understood as the result of two surface waves at both interfaces coupling either in phase or out of phase. The mode with the smallest fraction of the field inside the thin layer is the long-range mode, whereas the mode with the largest fraction of the field in the thin layer is the short-range mode. This field distribution gives rise to a stronger absorption in the last one and to a shorter propagation length [7].

In strongly absorbing thin films there are also long-range guided modes, which obey the dispersion relation given by Eq. (1). These modes result from the coupling of the evanescent fields at opposite side of the absorbing field, i.e., films with $|\varepsilon_{2r}| \lesssim \varepsilon_{2i}$ (independent of the sign of ε_{2r}) and $\varepsilon_{2i} \gg \varepsilon_1$. As we show next, short-range modes in thin absorbing layers, defined by Eq. (2), are leaky waves with a wave number smaller than the wave number of free space radiation in the surrounding dielectric.

We have calculated the real components of the complex propagation constant (β_{xr}) of guided modes in thin slabs of materials with permittivities $\varepsilon_2 = 20+1i$, $-20+1i$ and $1+20i$ in vacuum and at λ =600 nm. We choose these values based on the following classification of materials: Weakly absorbing dielectrics $(20+1i)$, weakly absorbing metals $(-20+1i)$ and strongly absorbing materials $(1+20i)$. These calculated values of the wave number are displayed in Fig. 1 as a function of the thickness of the layer normalized by λ, i.e., as a function of d/λ. The values of β_{xr} in this figure are normalized by the wave number in the surrounding dielectric $k_0 n_1$, where we set $n_1 = \sqrt{\varepsilon}_1 = 1$ as the refractive index of vacuum. For $\varepsilon_2 = 20+1i$ (Fig. 1(a)), β_{xr} corresponds to the conventional TM_0 mode in a planar dielectric slab. The LRSPPs and SRSPPs in the slab with $\varepsilon_2 = -20+1i$ are represented by the solid and dashed curves in Fig. 1(b). Figure 1(c) displays the calculation of long-range (solid curve) and short-range guided modes (dashed curve) in an absorbing layer with $\varepsilon_2 = 1+20i$. The dashed lines in Figs. 1(a), 1(b) and 1(c) correspond to the light line or the wave number of radiation in the surrounding medium.

Although we have derived the guided modes by thin slabs of arbitrary permittivity with the same set of equations (Eqs. (1)-(2)), we note that there are important differences between a generic TM_0 guided mode in a dielectric slab and long-range guided modes in a metal or absorbing layer. A conventional TM_0 mode is a bulk mode resulting from the interaction of the fields at the two surfaces of the thin film by means of total internal reflection; while long-range modes are guided modes due to the coupling between two surface modes at opposite interfaces penetrating the layer. This difference can be appreciated in Figs. 1(a), 1(b) and 1(c), where the wave number of the TM_0 mode in non-absorbing dielectric layers converges for large thicknesses to the value of free space radiation in the layer, while this wave number converges to the value of surface polaritons on single interfaces for the case of metals and strongly absorbing materials, i.e., $\beta_{xr} = (\omega/c)\mathrm{Re}[(\varepsilon_1\varepsilon_2)/(\varepsilon_1+\varepsilon_2)]$, where ω/c is the wave number in vacuum. We also note that the wave number of SRSPPs (Fig. 1(b)) increases for small thickness, while the wave number of LRSPPs converges to the value for free space radiation in the surrounding dielectric. This behavior indicates that LRSPPs are less confined to the thin layer and extend more into the surrounding dielectric as the thickness decreases, while the opposite behavior happens for SRSPPs. For the case of long-range and short-range guided modes in the thin absorbing layer (Fig. 1(c)), we see that in the thick film limit the wave number converges to the value of surface polaritons in single interfaces. This value is below the light line of the

#162216 - $15.00 USD Received 1 Feb 2012; revised 27 Mar 2012; accepted 27 Mar 2012; published 10 Apr 2012

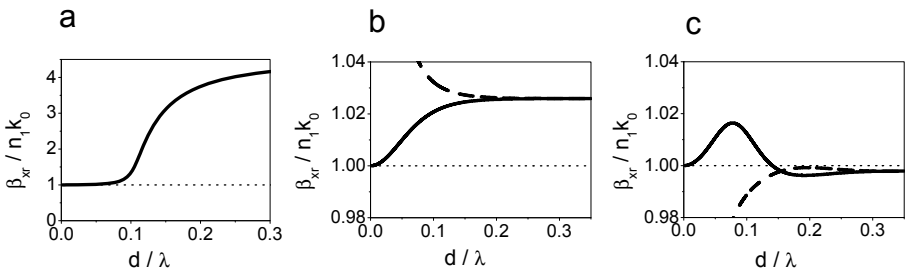

Fig. 1. Real component of the wave number β_{xr}, normalized to the wave number in the surrounding medium, $n_1 k_0$, of guided modes in a thin slab with (a) $\varepsilon_2 = 20 + 1i$, (b) $\varepsilon_2 = -20 + 1i$ and (c) $\varepsilon_2 = 1 + 20i$, as a function of the thickness of the layer normalized by the wavelength. The surrounding medium is considered to be vacuum. The dashed line indicates the normalized wave number of the surrounding medium.

surrounding dielectric because the real component of permittivity of the thin layer is positive. Therefore, these modes are leaky into the dielectric in contrast to surface plasmon polaritons on single interfaces. Long-range guided modes become surface modes, with wave number larger than that of the surrounding dielectric, for thicknesses below $d/\lambda = 0.14$ in the specific case shown in Fig. 1(c). We note that as the thickness is further reduced, the wave number of long-range modes converges to the light line as it was the case for LRSPPs. Short-range modes remain below the light line for any thickness indicating that these modes are not guided as they leak into the surrounding dielectric.

3. Long-range guided mode sensor based on a thin layer of chalcogenide glass

We have investigated long-range modes supported by thin layers of the amorphous chalcogenide glass $Ge_{17}Sb_{76}Te_7$. Chalcogenide glasses have a metallic (crystalline) and a dielectric (amorphous) phase, are inexpensive, present a strong optical absorption in the visible [19], are chemically stable and can be deposited in layers with nanometer accuracy [20]. These characteristics make chalcogenide glasses an excellent alternative to noble metals in sensing applications. We have determined the dielectric permittivity of amorphous GST (a-GST) and crystalline GST (c-GST) with ellipsometry measurements. The values of the permittivity are displayed in Figs. 2(a) and 2(b) for a-GST and c-GST, respectively.

The measurements shown below have been performed in samples of a-GST, in which the absorption coefficient is larger than 10^5 cm^{-1} in the visible. The permittivity of a-GST around

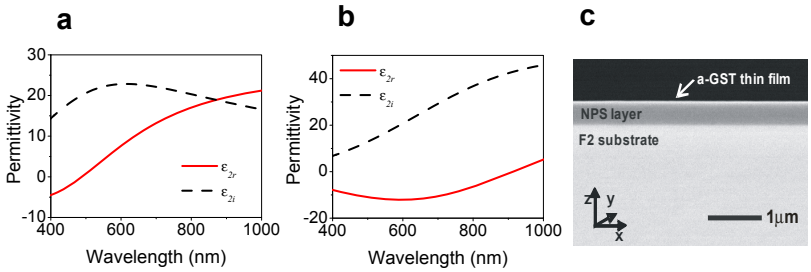

Fig. 2. Real and imaginary components of the permittivity of (a) a-GST and (b) c-GST as a function of wavelength. (c) Scanning electron microscope image of the cross section of a sample.

#162216 - $15.00 USD Received 1 Feb 2012; revised 27 Mar 2012; accepted 27 Mar 2012; published 10 Apr 2012

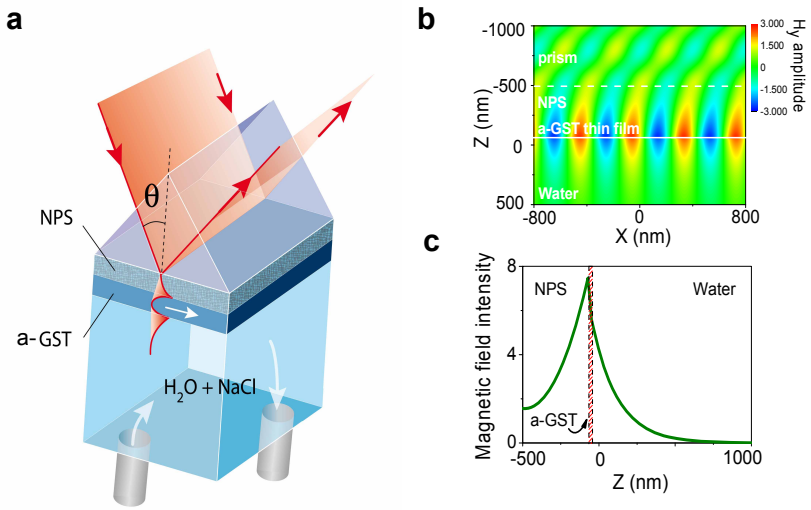

Fig. 3. (a) Schematic representation of the long-range mode sensor. A p-polarized plane wave is incident at an angle θ onto the interface separating a high refractive index prism and a layer of nanoporous silica. The evanescently transmitted amplitude can couple to a long-range guided mode by the a-GST layer. (b) Calculation of the magnetic field amplitude for p-polarized light ($\lambda = 530$ nm) incident at an angle of 56.6° with respect to the sample normal onto the multilayer shown in Fig. 2(c). The a-GST layer is exposed to water. The incident wave couples to a long-range guided mode on the a-GST layer at this wavelength and angle. The maximum field amplitude is at the interfaces of the a-GST layer. (c) Magnetic field intensity of the long-range mode across the different layers in the multilayer structure. The field intensity decays evanescently from the a-GST interface.

$\lambda = 500$ nm is close to the value of $\varepsilon_2 = 1 + 20i$ used in the example of the previous section. The sample is a multilayer structure formed by a Schott F2 glass substrate with a refractive index of 1.62, a layer of nanoporous SiOC:H (NPS) [21] with a thickness of 430 nm and a refractive index of 1.35 between 300 and 700 nm, and a layer of a-GST with a thickness of 20 nm. The NPS was spin coated onto the substrate, while the a-GST was deposited with electron beam sputtering. A side view scanning electron microscope image of a cleaved sample is displayed in Fig. 2(c). The sample was attached to a flow cell.

The excitation of long-range guided modes was achieved by using the attenuated total internal reflection method in the Kretschmann-Raether configuration. A schematic representation of this technique is displayed in Fig. 3(a). The polarization of the incident beam was set parallel to the plane of incidence, i.e., p-polarized. Figure 3(b) illustrates the coupling of the incident light to guided modes. This figure displays a calculation of the magnetic field amplitude in a sample with the parameters described above and water at the exposed side of the a-GST layer. A p-polarized plane wave is incident at an angle of 56.6°. This angle corresponds to the angle for resonant coupling to the long-range guided mode. The maximum field amplitude is at the surfaces of the a-GST layer, i.e., at $z = 0$ and $z = -20$ nm, and the field decays exponentially from these surfaces into the surrounding dielectrics (NPS and water). This exponential decay is also illustrated in Fig. 3(c), where the square of the magnetic field amplitude of the mode at $x = 0$ nm is plotted against the distance to the a-GST thin layer.

To determine the sensitivity of long-range guided modes to small changes in the refractive index of the surrounding medium, we have performed attenuated total reflectance measurements with a diode pumped laser emitting at $\lambda = 530$ nm by filling the flow cell with a solution of NaCl

#162216 - $15.00 USD Received 1 Feb 2012; revised 27 Mar 2012; accepted 27 Mar 2012; published 10 Apr 2012

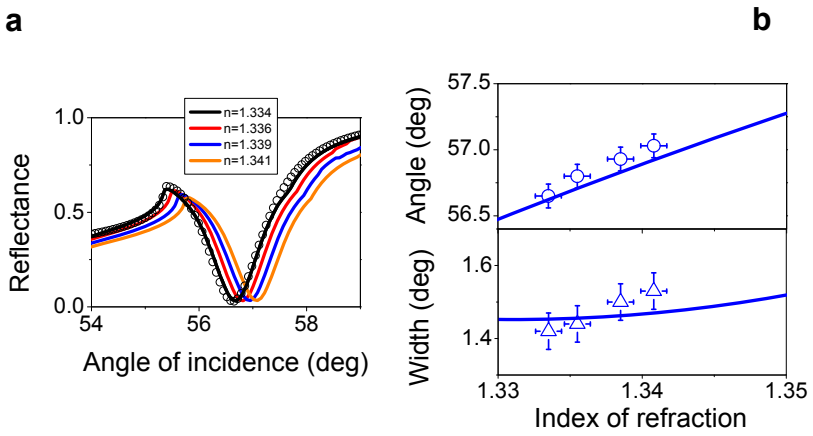

Fig. 4. (a) Attenuated total reflectance measurements of the multilayer shown in Fig. 2(c) at $\lambda = 530$ nm, exposed to various solutions with different refractive indices. A fit to the measurement with a solution of refractive index 1.334 is displayed with the black open circles. (b) Measured (symbols) and calculated (lines) resonance angles (circles) and widths (triangles) as a function of the refractive index of the solution.

in purified water [22]. Long-range guided modes arise from the coupling between evanescent waves at the opposite sides of the thin layer. This coupling is only possible when the dielectric media close to the thin layer on both interfaces have similar refractive index. In order to obtain this condition, the NPS layer was baked at 400°C for 30 minutes to increase its porosity and thereby decrease its refractive index to about 1.35. The F2 glass substrate was optically matched to the F2 prism with refractive index matching liquid. An optical beam was incident onto a F2 glass-NPS interface at an angle larger than the total internal reflection angle. The evanescently transmitted amplitude into the NPS layer can couple to a long-range guided mode in the a-GST layer at the resonant angle and frequency. The coupling to long-range modes is measured by detecting a reduction of the specular reflectance at the F2 glass-NPS interface. A reference for the reflection was obtained by measuring the total internal reflection of s-polarized light. The reflectance is 1 for this polarization and for angles of incidence larger than the critical angle.

Figure 4(a) shows the reflectance as a function of the angle of incidence. The reduction of the total internal reflectance corresponds to the resonant excitation of long-range modes in the a-GST thin layer. The measurements were fitted to calculations based on Fresnel's coefficients for the multilayer structure. For clarity, we only plot one fit in Fig. 4(a) with the black open circles. Similar fits were obtained for the different samples. The long-range mode resonance shifts to larger angles and broadens when the concentration of NaCl increases.

The resonance angle θ_r, defined as the angle of the minimum of reflectance, and resonance width $\Delta\theta_r$, defined as the width of the resonance at a reflectance of 50%, are plotted as a function of the refractive index of the surrounding solutions in Fig. 4(b) with open circles and triangles respectively. The solid lines in this figure correspond to calculations for the multilayer structure. The resonance shifts to larger angles as the refractive index of the aqueous solution increases is due to the modification of the phase matching condition and the resonant coupling between the incident plane wave and the long-range guided mode. The increase in resonance width is a consequence of the difference in refractive index between the NPS layer and the water-NaCl solution. This difference weakens the coupling between the surface waves at the opposite interfaces of the a-GST layer, leading to an increase of the penetration of the electromagnetic field into the absorbing a-GST layer and to a stronger absorption.

#162216 - $15.00 USD Received 1 Feb 2012; revised 27 Mar 2012; accepted 27 Mar 2012; published 10 Apr 2012

The figure of merit of the sensor is defined as $FoM = \frac{\delta\theta_r}{\delta n}\frac{1}{\Delta\theta_r}$, [23–26] where $\delta\theta_r$ is the shift of the resonance angle due to a change in the refractive index of the solution δn. For the investigated sample at $\lambda = 530$ nm the *FoM* is 52 in inverse RIU's [27].

4. Characteristic parameters of long-range guided mode sensors

To compare the intrinsic properties of different surface modes for sensing, we have calculated the modification of their complex propagation constant, $\beta_x = \beta_{xr} + i\beta_{xi}$, due to changes in the refractive index of the surrounding medium. In contrast to the *FoM* given in the previous section, the influence of the method used to couple the incident light to the surface modes is not considered here, facilitating a general comparison of surface modes for sensing.

Two parameters should be taken into account in order to characterize the performance of optical sensors: The intrinsic sensitivity *IS*, and the decay length L_z of the evanescent field in the surrounding medium [3]. The intrinsic sensitivity is defined as the derivative of the real component of the propagation constant with respect to the refractive index of the surrounding medium normalized by the imaginary component of the propagation constant,

$$IS = \frac{\delta\beta_{xr}}{\delta n}\frac{1}{\beta_{xi}}\,. \tag{3}$$

The decay length L_z defines the dimensions of the surrounding medium in contact with the layer that influence the resonance. This length is given by

$$L_z = \frac{1}{2Re(\sqrt{\beta_x^2 - k_0^2 n_1^2})}\,. \tag{4}$$

The propagation constant β_x can be obtained from Eq.(1), where we use the permittivity of Au given in Ref. [28], and the measured permittivities for the GST.

The intrinsic sensitivity *IS* and decay length L_z of long-range guided modes supported by a thin layer of a material with complex permittivity $\varepsilon = \varepsilon_{2r} + i\varepsilon_{2i}$ surrounded by a dielectric with a refractive index of $n_1 = 1.33$ are represented in Figs. 5(a) and 5(b) respectively with the color scale, as a function of ε_{2r} and ε_{2i}. For these calculations, we consider a layer with a thickness d and a wavelength λ such that $d/\lambda = 0.038$. This is the same thickness-to-wavelength ratio as in the measurements of the previous section. To obtain a good contrast in the figures, we have fixed the maximum of the color scale of Fig. 5(a) at 500, and of Fig. 5(b) at 0.6. The symbols display the values of *IS* and L_z for a thin film of gold (squares), a-GST (circles) and crystalline c-GST (triangles) for wavelengths varying from 400 nm to 650 nm in steps of 19 nm. The values of *IS* and L_z in Figs. 5(a) and 5(b) at different wavelengths correspond to layers with a thickness $d = 0.038\lambda$.

It is interesting to discuss the different regions in Figs. 5(a) and 5(b): The white areas close to the origin corresponds to the permittivity for which thin layers can not support guided modes. On the right-bottom part of the graphs we have layers of weakly absorbing dielectrics ($\varepsilon_{2r} > \varepsilon_1, \varepsilon_{2i} \ll \varepsilon_{2r}$) that support TM_0 modes that are guided by total internal reflection. These modes provide a large *IS* due to a very narrow resonance that results from the weak absorption in the layer. However, the field decays a long distance in the surrounding medium, i.e., L_z is large, which limits the applicability of these materials for the detection of small molecules. On the left-bottom part of Figs. 5(a) and 5(b) there is the region of low-loss metals that support long-range surface plasmon polaritons, i.e., $-\varepsilon_{2r} > \varepsilon_1, \varepsilon_{2i} \ll |\varepsilon_{2r}|$. Long-range surface plasmon polaritons combine a large *IS* and a very good confinement ($L_z/\lambda \ll 1$). However, there is a very limited choice of materials with a permittivity that fullfills these characteristics [2]. In the case of Au (blue squares), the *IS* is large at long wavelengths, but it decreases rapidly below

#162216 - $15.00 USD Received 1 Feb 2012; revised 27 Mar 2012; accepted 27 Mar 2012; published 10 Apr 2012

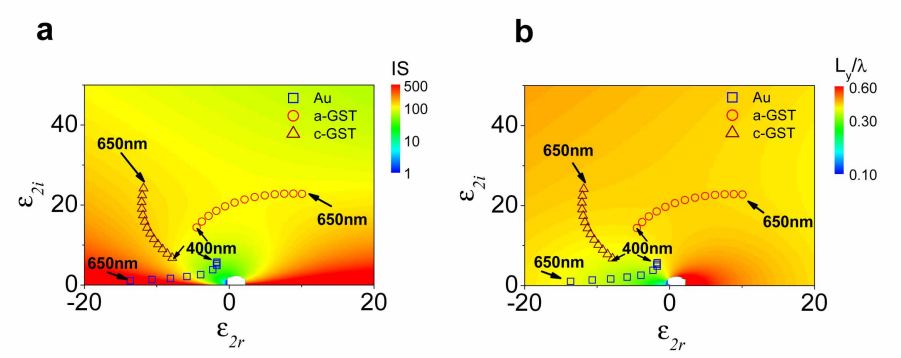

Fig. 5. (a) Calculated intrinsic sensitivity and (b) decay length normalized to the wavelength of long-range guided modes in a layer with a thickness d and at wavelength λ such that $d/\lambda = 0.038$, plotted as a function of the real and imaginary components of the permittivity of the thin layer. The surrounding medium has a refractive index of 1.33. The open symbols indicate the permittivity of Au (squares), a-GST (circles) and c-GST (triangles) at different wavelengths equally spaced between 400 (innermost symbols) and 650 nm (outermost symbols). The IS and L_z/λ values indicated by the symbols correspond to layers with a thickness to wavelength ratio d/λ =0.038.

$\lambda = 550$ nm. Besides the limits of weakly absorbing dielectrics and low-loss metals, there is the wide region of permittivities that characterize long-range guided modes, i.e., $\varepsilon_{2i} \geq |\varepsilon_{2r}|$. Note that as long as $|\varepsilon_{2r}| \ll \varepsilon_{2i} < 30$, the IS is improved when ε_{2i} increases, i.e., when the optical loss in the thin film increases. This is a surprising result, which can be understood as follows: The energy density inside the thin absorbing film is reduced when the optical loss increases due to the coupling and interference of surface waves at the opposite sides of the layer [13]. This reduction of the field minimizes the losses of long-range guided modes, narrowing the resonance and improving the IS. We can notice in Fig. 5(a) that chalcogenide thin layers have a better IS than gold at shorter wavelengths than $\lambda = 550$ nm. In the case of dielectrics ($\varepsilon_{2r} > 0$), L_z is first reduced as ε_{2i} increases, but it increases for large ε_{2i}. For metals ($\varepsilon_{2r} < 0$), L_z increases as ε_{2i} increases.

The coupling strength between modes at the opposite sides of the thin layer depends on its thickness, d. Therefore, a change in d will have an impact on the IS and L_z. The dependency of this parameter from d =5 to 40 nm and at λ =500 nm is illustrated in Figs. 6(a) and 6(b) for Au (blue-dotted curve), a-GST (red-solid curve) and c-GST (green-dashed curve). The thinnest layer of 5 nm for these calculations is justified by the possibility of depositing such thin layers of chalcogenide glasses [20]. However, we have to point out that metal films with this thickness are challenging to fabricate [7]. This characteristic constitutes an important advantage of chalcogenide glasses over metals for long-range surface wave sensing. The IS is improved and L_z increases as d decreases. This behavior is due to the stronger coupling of modes at opposite interfaces, which leads to a reduction of the mode energy density in the thin layer of lossy material and longer extension of the field in the surrounding medium.

In Figs. 6(c) and 6(d) we have plotted the IS and L_z of a-GST (solid curve) and c-GST (dashed curve) thin layers normalized by the respective values for Au layers as a function of d for λ=500 nm. A four-fold improvement of the IS can be achieved by using GST films with a thickness below 10 nm, while maintaining similar confinement of the field to the layer. We stress that the fabrication of films of Au with a thickness of 10 nm or thinner is very challenging. Therefore, the maximum IS attainable with GST films may be more than one

#162216 - $15.00 USD Received 1 Feb 2012; revised 27 Mar 2012; accepted 27 Mar 2012; published 10 Apr 2012

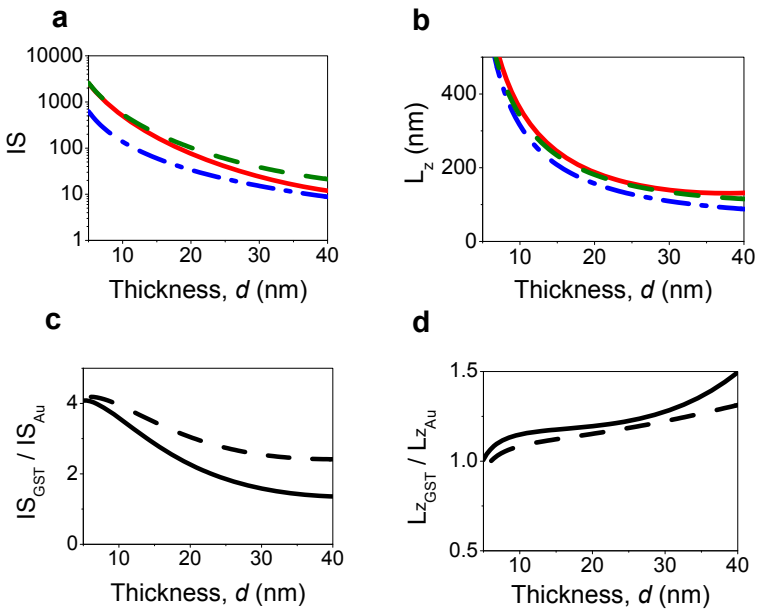

Fig. 6. (a) Calculated intrinsic sensitivities and (b) decay lengths of long-range guided modes at λ =500 nm in a layer of Au (blue-dashed-dotted curve), c-GST (green-dashed curve) and a-GST (red-solid curve) as a function of the thickness of the layer. (c) Intrinsic sensitivity and (d) decay length ratios between a layer of a-GST or c-GST and Au (solid and dashed curves respectively) at $\lambda = 500$ nm as a function of the thickness of the layer. The thin layer is surrounded by a medium with a refractive index of 1.33.

order of magnitude larger than the maximun experimentally attainable *IS* with thin metal films. Furthermore, the decay length can be adjusted by the thickness of the layer. This tuneability of L_z will allow the optimization of the sensitivity to species with different sizes by improving their spatial overlap with the electromagnetic field.

In order to compare the characteristic parameters of the sensors at different wavelengths in the visible, Figs. 7(a) and 7(b) display the *IS* and L_z of a-GST (red-solid curve), c-GST (green-dashed curve) and gold (blue-dashed-dotted curve) as a function of λ in the range 400 to 630 nm. The *IS* and L_z of long-range guided modes in a-GST and c-GST normalized by that of Au are displayed in Figs. 7(c) and 7(d) with a solid and dashed curve respectively. These curves have been obtained for layers with a thickness of 20 nm, i.e., the thickness of the layer used in the experiments shown in the previous section. The upper wavelength limit used in the calculations represents the wavelength typically used in Au surface plasmon resonance sensors. At this wavelength, Au sensors combine a high intrinsic sensitivity and a good field confinement. The *IS* of chalcogenide layers with a thickness of 20 nm is ~ 5.5 times lower than that of gold layers at 630 nm. However, this *IS* ratio between chalcogenide and Au sensors increases significantly as the wavelength is reduced, mainly due to the reduced performance of Au as interband absorption becomes more important. The *IS* of an a-GST sensor is 2.4 times better than that of an Au sensor at 500 nm. This *IS* is further improved with a c-GST sensor. As the wavelength is reduced also L_z decreases from 270 nm in the case of Au at $\lambda = 630$ nm to about 190 nm for the chalcogenide glasses at $\lambda = 500$ nm. This reduction of L_z is relevant for the detection of small molecules bounded to the surface of the thin layer. Therefore, we can state that long-range guided modes supported by strongly absorbing thin layers improve the *IS* of Au SPR sensors at short wavelengths allowing for a better confinement of the electromagnetic field

#162216 - $15.00 USD Received 1 Feb 2012; revised 27 Mar 2012; accepted 27 Mar 2012; published 10 Apr 2012

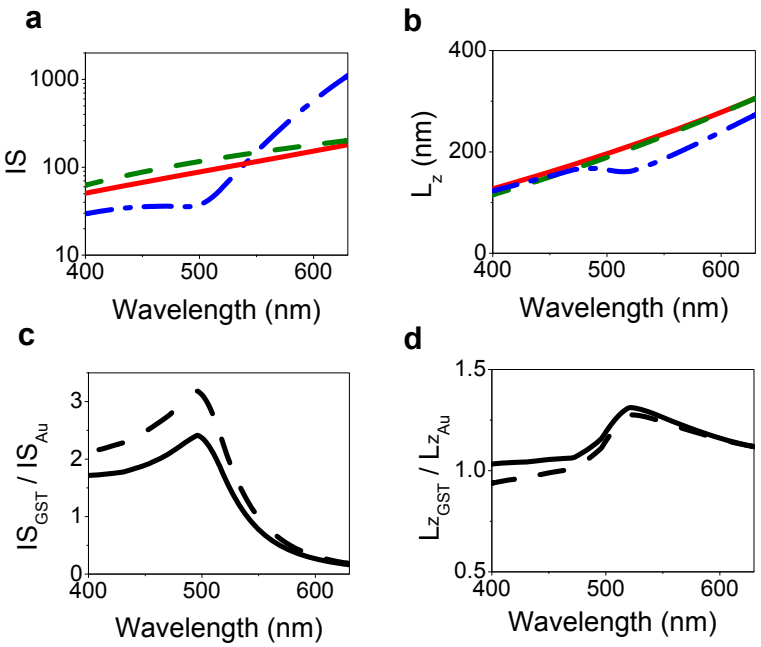

Fig. 7. (a) Calculated intrinsic sensitivities and (b) decay lengths of long-range guided modes in a layer of Au (blue-dashed-dotted curve), c-GST (green-dashed curve) and a-GST (red-solid curve) with a thickness of 20 nm as a function of the wavelength. (c) Intrinsic sensitivity and (d) decay length ratios between a layer of a-GST or c-GST and Au (solid and dashed curves respectively) as a function of the wavelength. The thin layer is surrounded by a medium with a refractive index of 1.33.

to the thin layer.

5. Conclusions

We have demonstrated that strong optical absorption in materials is not a limitation for the sensitivity of surface wave sensors. In particular, we have shown that long-range guided modes supported by nanometric films of strongly absorbing chalcogenide glasses can be used as sensitive probes of changes in the refractive index of the surrounding medium. Our results open a new range of possibilities for surface wave sensing using different substrates and operating at shorter wavelengths, thereby reducing the decay length of the field from the surface. A larger field confinement can be exploited to increase the sensitivity to changes in functionalized surfaces.

Acknowledgments

We acknowledge M. Maas, H. de Barse, A.P.M. de Win and H. Herps for technical assistance during sample fabrication and characterization and M. Verschuuren, V. Giannini and M. Forcales for discussions. This work was supported by the Netherlands Foundation Fundamenteel Onderzoek der Materie (FOM) and the Nederlandse Organisatie voor Wetenschappelijk Onderzoek (NWO) and it is part of an industrial partnership program between Philips and FOM.

#162216 - $15.00 USD Received 1 Feb 2012; revised 27 Mar 2012; accepted 27 Mar 2012; published 10 Apr 2012